Colorimetric Plasmon Resonance Imaging Using Nano Lycurgus Cup Arrays

*Manas Ranjan Gartia, Austin Hsiao, Anusha Pokhriyal, Sujin Seo, Gulsim Kulsharova, Brian T. Cunningham, Tiziana C. Bond, and Gang Logan Liu**

Lycurgus cup[1] created by ancient Romans 2000 years ago can appear different colors depending on the direction of light illumination in which it is viewed due to metal nanoparticle optical scattering. It has inspired nanoplasmonics research over the past decade.[2–5] Here we present a nanoscale Lycurgus cup arrays (nanoLCA) device that has the property of appearing green when light is shone on to it and changing the color to red without direct light illumination (see Supporting movie). The above colorimetric device fabricated on transparent plastic substrate consists of about one billion nano Lycurgus cups in an array with subwavelength opening and decorated with metal nanoparticles on side walls. Strikingly different from metallic nanohole arrays[6] or quasi-3D plasmonic crystals[7] with extraordinary optical transmission which usually give rise to multiple transmission spectral features, nanoLCA exhibits metal nanoparticle-like single transmission wavelength peak in the whole visible ranges. Electromagnetic simulation revealed the plasmon resonance scattering modes of the metal nanoparticles on the cup side walls and the corresponding single peak wavelength scattering light selectively transmitted by the nanoLCA. The huge transmission and reflection wavelength shifts upon binding of molecules on our flexible, high-throughput, large area nanoLCA device are up to 200 nm (with maximum sensitivity of 46000 nm per refractive-index unit (RIU) and figure of merit (FOM) of 1022), much greater than the typical nanoparticle plasmon resonance wavelength shift and large enough to detect the color differences directly by naked eyes and conventional bright field microscopes. This enables to eliminate the need for precision spectrometer or fluorescence labeling. We demonstrated the ultrasensitive label free colorimetric plasmon resonance imaging of different refractive indices solutions, single and double stranded oligonucleotides and antigen-antibody protein interactions on our nanoLCA device.

With the advancement of nanoscale fabrication, label-free sensors such as photonic crystal,[8] whispering gallery mode (WGM)[9] and surface plasmon resonance (SPR)[5] based devices are increasingly being used for detecting DNA bases, recognizing antigen-antibody, probing protein interaction, immunoassays and identifying pathogen. Most of the above sensors work on the principle of shift in the resonance wavelength after conjugation of biomolecules to the surface of the sensor. However, the resonance peak wavelength shift (PWS) for most of the current sensors is of the order of few nanometers only[9,10] (although SPR has much higher sensitivity of 2×10^6 nm per RIU[11] for bulk refractive index, the absolute change in wavelength is extremely minimal for commercial SPR sensor in Kretschmann configuration).[11,12] Hence, the identification of the unknown analyte (or concentration of a known analyte) requires specialized instrument such as high precision spectrometer, multiplexer for sweeping the laser wavelengths, WGM trap, complex optical system to generate SPR (for example, prism, accurate angle tuning for the optical beam) etc. Localized surface plasmon resonance (LSPR) sensors,[5] based on colloidal plasmonic particles (silver, gold), overcome some of the above limitations. However, the sensitivity of LSPR based sensors are at least an order of magnitude less compared to the gold standard prism coupled SPR sensors (Kretschmann configuration).[13] In LSPR configuration,

Prof. G. L. Liu
Department of Electrical and Computer Engineering
University of Illinois at Urbana-Champaign
Urbana, Illinois, 61801, USA
E-mail: loganliu@illinois.edu
M. R. Gartia
Department of Nuclear, Plasma and Radiological Engineering
University of Illinois at Urbana-Champaign
Urbana, Illinois, 61801, USA
Dr. T. C. Bond
Meso, Micro and Nano Technologies Center
Lawrence Livermore National Laboratory
7000 East Avenue, Livermore, California, 94550, USA
Prof. B. T. Cunningham, Prof. G. L. Liu
Department of Bioengineering
University of Illinois at Urbana-Champaign
Urbana, Illinois, 61801, USA
A. Pokhriyal
Department of Physics
University of Illinois at Urbana-Champaign
Urbana, Illinois, 61801, USA
S. Seo
Department of Material Science and Engineering
University of Illinois at Urbana-Champaign
Urbana, Illinois, 61801, USA
G. Kulsharova, Prof. B. T. Cunningham, Prof. G. L. Liu
Department of Electrical and Computer Engineering
University of Illinois at Urbana-Champaign
Urbana, Illinois, 61801, USA
M. R. Gartia, A. Hsiao, A. Pokhriyal, S. Seo, G. Kulsharova,
Prof. B. T. Cunningham, Prof. G. L. Liu
Micro and Nano Technology Laboratory
University of Illinois at Urbana-Champaign
Urbana, Illinois, 61801, USA

DOI: 10.1002/adom.201200040

the scattering spectra of the plasmonic particles shift to a different wavelength (usually to a longer wavelength) after conjugation to specific analytes. However, the colloid particle sizes and positions are random and difficult to control over a large area. Thus, in the same sample area, different particles give rise to different scattering spectra and hence, for the same analyte the shifts in the wavelength are different.[5] In addition, a high precision spectrometer is required to record the spectra and then complex image analysis is required to extract usable data. Although related to the field of plasmonics, label free sensor such as surface enhanced Raman spectroscopy (SERS) based techniques are not discussed here.

Another method to get high sensitivity plasmonic resonance is to make sub-wavelength holes in optically thick metal surfaces. This is also commonly known as extraordinary optical transmission (EOT) substrates.[6,14] The fabrication of such substrates relies on expensive, time consuming and low throughput electron beam lithography and focused ion beam milling. Also, due to presence of single layer of metal surface, usually the nonradiative Drude (ohmic) damping losses are high, leading to damping of resonance with analytes on the top of the metal surface.[15] In addition, EOT substrates generally show multiple transmission peaks in the visible range, making it difficult for true colorimetric sensing modalities.[6] Quasi 3D plasmonic crystals[7] offer a way to increase the sensitivity by employing multiple layers of metal surfaces on nanohole surface. But mostly the resonance of such device has been demonstrated in near infrared and far infrared wavelength. Also, after adsorption of analyte, no shift (or minimal shift) in the resonance was observed. Most of the analyte detection or quantification was done from the change in the infrared transmission intensities.

In contrast, we employ a nanoimprint method to produce nanoLCA substrate on plastic substrate to reduce cost and simplify the fabrication process. Metal (Ag or Au) was deposited on the nanoLCA by electron beam evaporation, producing metal surface on the rim of the holes, on the bottom of the holes and also nanoparticles-like structure on the sidewalls of the holes. Due to selective transmission of the scattering spectra from the nanoparticles, our device is characterized by single transmission spectral peak in the entire visible wavelength, giving rise to the Lycurgus cup effects (see Supporting movie). Due to unprecedented high sensitivity (about 46000 nm per RIU), nanoLCA device is very sensitive in detecting small changes in refractive index of the analyte and gives rise to a huge shift in the resonance wavelength which is even detectable by naked eyes and normal bright field (BF) microscopy making it a true colorimetric sensor.

Figure 1a depicts the schematic of the nanoLCA structure. As shown in the inset, it consists of nanofunnel shaped cup structure decorated with multiple nanoparticles along the side walls. The master nanocone pattern is first fabricated on a glass substrate using laser interference lithography technique[16,17] with a range of different heights (h = 250, 500 and 1000 nm) (see Figure S1 in Supporting Information). We successfully transferred the two-dimensional square lattice of nanoLCA (pitch, p = 350 nm) to a flexible and optically transparent polyethylene terephthalate (PET) film using nanoreplica molding process (see Experimental Section and Supporting Figure S2). In order to make the structure surface plasmon active, we deposited different thickness, t, of silver metal layer (t = 40, 60, 70, 80, 90, 100 and 120 nm). In order to demonstrate the apparent analogy to Lycurgus cup, Figure 1b shows optical image of the fabricated nanoLCA structure coated with metal (t = 90 nm) with (left) and without (right) direct illumination of white light, respectively. The scanning electron micrograph (SEM) of the nanoLCA (30° tilt and cross-sectional) is given in Figure 1c. The metal nanoparticles on the sidewall of nanoLCA are quite apparent from the SEM images. In the paper, we will focus on the results obtained from nanoLCA with height, h = 500 nm; diameter, d = 180 nm and metal film thickness, t = 90 nm; and pitch, p = 350 nm as it showed better sensitivity and narrow spectral resonance features (compared to h = 1000 nm). Due to strong interaction between surface plasmon and molecules near metal surface, surface plasmon based sensor has been widely used to exploit the plasmon-molecule interaction.[18] One of such modalities is the refractive index sensing using surface plasmon for molecules that have no (or minimal) optical absorption or that has electronic absorption energies far away from the surface plasmon resonances. To illustrate the point, we have demonstrated the refractive index sensing using fourteen different chemicals with varying refractive indices (n = 1.333 – 1.56). As shown in Figure 1d (top image is transmission mode and bottom image is reflection mode), the transmitted light through the nanoLCA changed from light blue to green and to red with gradual increase in the refractive index. For example, the intensity of Red channel increased to 208 (Immersion oil, n = 1.51) from 18 (Air, n = 1). The reflection images also showed large shift in color (from red to light green) upon the gradual increase of refractive index. Since the surface plasmon resonance peak shift is large (~100 nm) after changing the refractive index environment of the superstrate, it is possible to distinguish the chemicals from the colorful transmission images. **Figure 2**b shows the mean red channel intensity (see Experimental Section for the RGB analysis) derived from the images shown in Figure 1d. We have also implemented the Earth Mover Distance (EMD) algorithm (see Experimental Section) to compare how much the image with varying RI environment are different from that of image with water environment.

In view of large shift in the resonance wavelength due to higher sensitivity of our sensor, we can monitor the refractive index change from the BF transmission/reflection images using a simple optical microscope with a white light source. Figure 1e depicts structured illumination of nanoLCA using photo lithographically patterned "NANO" and "ILLINOIS" mask. White light is illuminated from below the mask, but only green light passes through the nanoLCA sensor and collected by the charge coupled device (CCD) detector of the microscope. After putting ethanol (refractive index, n = 1.362) on the "IL" part of the word "ILLINOIS", the color changes from light blue to yellow. Similarly, the transmitted color changed from light blue to green and red for water and immersion oil respectively. The vibrant color created after mixing of 15% NaCl (middle orange), immersion oil (red), and ethanol (yellow) on the nanoLCA device is also shown in Figure 1e.

Figure 2a shows the spectroscopic results of the refractive index sensing on the nanoLCA structure. The zeroth order transmission spectrum for Ag-air interface (n = 1) reveals a bulk plasmon peak (Supporting Figure S3) for silver at λ = 320 nm.[19]

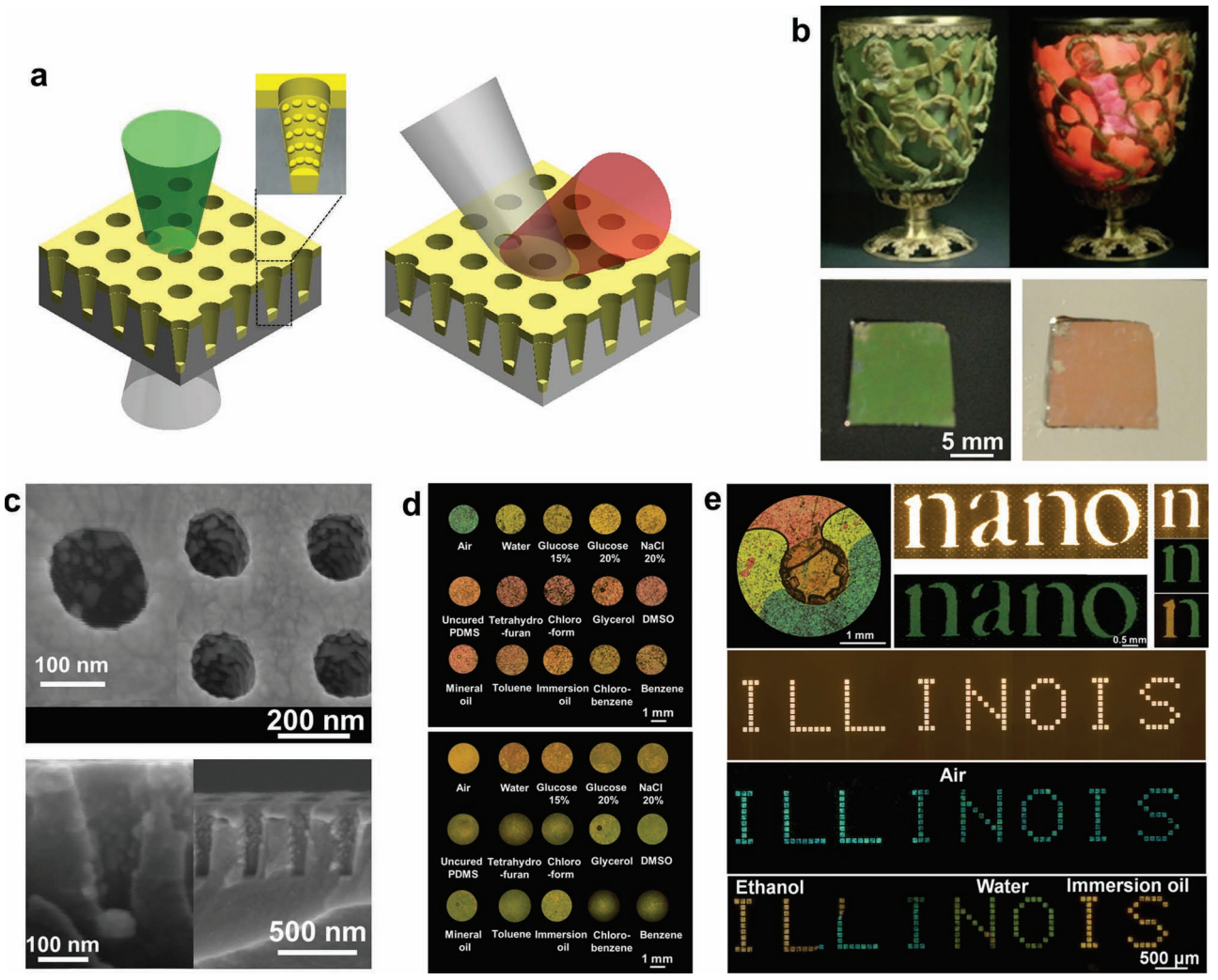

Figure 1. Refractive-index imaging with nano Lycurgus cup arrays. (a) Schematic showing the nanoLCA; inset shows the nanoparticles along the sidewalls of the cup. The schematic also shows that green light is transmitted and red light is reflected by nanoLCA in transmission and reflection imaging modes in microscope respectively. (b) The Lycurgus cup in British Museum dated back to fourth century AD. Due to scattering of nanoparticles on sidewall (5–60 nm in diameter), the cup appears green in reflected light and appears red in transmission light. Optical micrograph of nanoLCA taken using a camera under direct illumination (green) and without illumination (red) of Xenon lamp flashlight. (c) 30° tilt and cross-sectional (bottom) view SEM images of nanoLCA. (d) Optical transmission mode (top) and reflection mode (bottom) images of nanoLCA with fourteen different chemicals with varying refractive indices. (e) Creation of vibrant colors in transmission mode image of nanoLCA with mixture of NaCl, immersion oil and ethanol. The word 'NANO' was printed on a transparency sheet and nanoLCA device was kept on top of it. Light was illuminated from the bottom of the transparency. An ethanol drop was placed on part of the letter 'N' which appears orange in the transmission image. The rest of the letter is green due to the transmission property of nanoLCA. To illustrate the high spatial control, a lithography mask in quartz with the word 'ILLINOIS' was made and light was transmitted from the bottom of the mask while the nanoLCA sitting on top of it. The color appears green with air interface but changes to orange, light green and red for ethanol, water and immersion oil interfaces respectively.

The peak at λ = 381 nm is due to surface plasmon polariton-Bloch wave (SPP-BW) (1,0) mode at Ag-air interface (n = 1). The SPP-BW and Wood's anomaly (WA) (due to the diffraction of light parallel to the surface)[20,21] for a rectangular lattice structure can be approximately calculated using the relation[7,21]

$$\lambda_{SPP-BW} = \frac{p}{\sqrt{i^2 + j^2}} \sqrt{\frac{\varepsilon_{Ag}(\lambda)\varepsilon_d}{\varepsilon_{Ag}(\lambda)+\varepsilon_d}} \quad (1)$$

$$\lambda_{WA} = \frac{p}{\sqrt{i^2 + j^2}} \sqrt{\varepsilon_d} \quad (2)$$

where, i and j are the order of SPP-BW or WA. The dip at λ = 350 nm is due to (1,0) WA at Ag-air interface. The intense peak at λ = 450 nm cannot be predicted by any lowest order SPP-BW or WA from the calculation (Supporting Figure S4). However, using Mie scattering calculation (see Experimental Section), we found that the peak at λ = 450 nm is due to the scattering from Ag nanoparticles with diameter d = 50 nm in PET environment

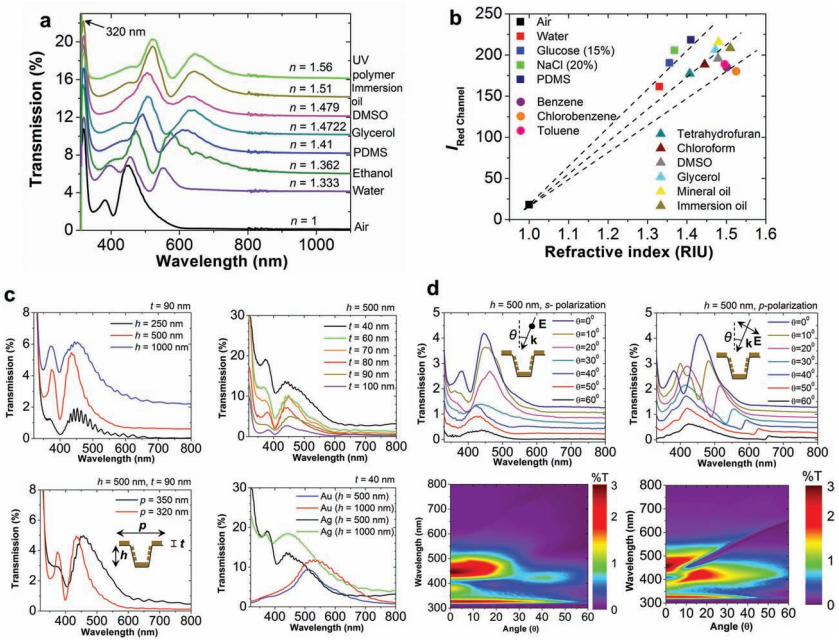

Figure 2. Optical properties of nanoLCA. (a) Zero-order transmission spectra of nanoLCA (h = 500, p = 350 and t = 90 nm) with different refractive index chemicals. (b) Variation of averaged red channel intensity with refractive-index. (c) Zero-order transmission spectra of nanoLCA with different height of nano cup, h = 250 nm (black), h = 500 nm (red), and h = 1000 nm (blue). For all the devices the thickness of Ag was t = 90 nm. To its right, figure shows the zero-order transmission spectra for nanoLCA with different Ag thickness (t = 40-100 nm). For all the devices the height of nano cup was h = 500 nm. Zero-order transmission spectra of nanoLCA device with two different pitch of nano cup, p = 320 nm (red), p = 350 nm (black). The transmission spectrum red shifted with increase in the pitch. Zero-order transmission spectra with Ag (40 nm) and Au (40 nm) for two different height of nano cup (h = 500 nm and h = 1000 nm). (d) Measured transmission spectra of nanoLCA in s-polarized and p-polarized light. The incident angle was varied from $\theta = 0°$ to $\theta = 60°$. The corresponding dispersion curve for each polarization is also presented as a contour plot. For plotting the contour plot, the angle of incidence was varied with an increment of 1°.

(n = 1.56) (See the dispersion diagram in Supporting Figure S5). Upon changing the refractive index of the superstrate from air (n = 1) to higher refractive indices solutions, the result showed that the bulk plasmon peak at λ = 320 nm remains unchanged (Figure 2a); the SPP-BW and WA features are red shifted, and the Mie scattered LSPR peak was red shifted by 100 nm for water (n = 1.333) and by almost 200 nm for immersion oil (n = 1.51).

The asymmetric nature of the spectrum also indicates the interference between SPP-BW, WA and scattered light from the nanoparticles transmitted by the nanoholes (see the Fano fitting in Supporting Figure S6). Since the boundary conditions and interfaces at each side of the metal (metal-substrate (n = 1.56) and metal-superstrate (e.g. n = 1)) are different and each side of the nanoLCA can support excitation of surface plasmon, the asymmetric structure leads to two sets of transmission peaks.[22] However, the intensity of the Mie scattered peak is much stronger than the supported SPP-BW peaks and hence, only single color is being transmitted by the nanoLCA structure. It should be noted that, the index-matching layer (n = 1.56) covering the nanoLCA structure leads to similar coupling efficiency for the two modes and manifested in transmission peaks of similar intensities (Figure 2a).

Further detailed optical characterization was carried out to reveal the property of nanoLCA. Figure 2c demonstrates the ability to control the resonance peak position by changing the height, h, and the pitch, p independently. The transmission intensity can be tuned by changing the metal thickness, t. The Q-factor of the sensor can be tuned (Supporting Figure 7 for reflectance measurement) by changing the height of the hole 'h'. The peak position can also the tuned by changing the hole diameter (by employing different RI UV cure polymer during the replica molding process). The angular and polarization dependent property of nanoLCA is shown in Figure 2d. In normal transmission ($\theta = 0°$), the transmission spectrum show two pronounced peaks at λ = 381 nm and λ = 450 nm. However, with increasing angle of incidence from $\theta = 0°$ to $\theta = 600$, the intensity of peak at λ = 381 nm gradually decreases for s-polarization. Also, the peak at λ = 450 nm blue-shifted to higher energy upon increasing the incident angle for s-polarization. However, for p-polarization both the peaks at λ = 381 nm and λ = 450 nm shifted to lower energy (red shifted) with the increase in incidence angle. Also, for p-polarization, the coupling to SPP-BW becomes much stronger than the LSPR modes with increasing the angle of incidence. The appearance of λ = 450 nm peak for s-polarization gives further indication that the peak at λ = 450 nm is a LSPR peak as SPP should not be excited efficiently by s-polarized incident light.[23]

To further understand the physics behind the experimental observations, full 3D finite difference time domain (FDTD) simulations are performed. To highlight the importance of cup shape and the side wall nanoparticles, we have simulated five different nanohole shapes (labeled 1–5) in **Figure 3**a. As expected nanohole without metal film on the sidewalls and continuous metal film on the side walls (similar to quasi 3D plasmonics crystal or EOT structures) shows multiple transmission peaks in the simulation (case 1–3) and do not match with the experimental observations. However, with incorporation of discrete metal film on the sidewalls and multiple particle-like structures (case-4 and 5) as the analogy to the Lycurgus cup, we started to observe similar peak features as in the experiment (the slight discrepancy in the experiment and simulations are due to the difficulties in exactly simulating the randomly decorated nanoparticles on the wall). The intense peak at λ = 450 nm is due to the LSPR mode at the gap between the nanoparticles and at the rim of the nanoLCA. The corresponding variation in the electric field intensity ($|E|^2$) is shown in Figure 3b. The top (X-Y) and cross-sectional (X-Z) views of the intensity distribution represents the electric field enhancement ($Log|E/E_{inc}|^2$) associated with the corresponding plasmon resonances. The LSPR mode of the particle at Ag-PET interface at λ = 450 nm is clearly visible in Figure 3b. The

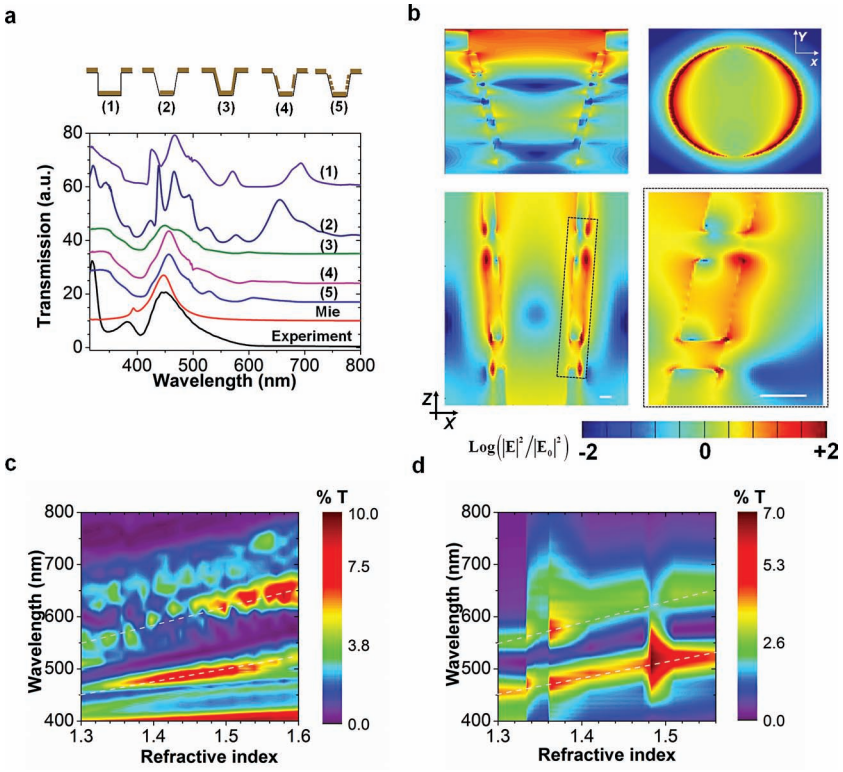

Figure 3. FDTD simulation for nanoLCA. (a) FDTD simulated transmission spectra for different shaped nanohole plasmonic device labeled (1)-(5). For all the simulations, h = 500 nm, t = 90 nm. The experimental transmission spectrum (black line) and calculated extinction spectrum for a nanoparticle (d = 50 nm) in a surrounding refractive-index of n = 1.56 (red line) is also presented. (b) Electric field distribution for nanoLCA; the cross-sectional (X-Z), top (X-Y) and sidewall nanoparticles zoom (X-Z) electric field distribution are shown. (c) FDTD simulated contour plot showing the variation of transmission spectra by changing the refractive index (RI) of surrounding medium for nanoLCA. The result showed appearance of two distinct peaks with increasing RI. Also, the first peak red-shifted from λ = 450 nm to λ = 525 nm and the second peak is red-shifted from λ = 550 nm to λ = 650 nm with the increase of RI. (d) Experimentally obtained contour plot showing the variation of transmission spectra of nanoLCA in presence of different RI liquids. The experimental contour plot showed remarkable resemblance to the FDTD simulated contour plot with appearance of two distinctive peaks and similar red-shift of resonance peaks.

cavity mode (SPP-BW) can also be found in Figure 3b. Detailed near-field intensity distribution for nanoLCA for different environment is presented in Supporting Figure S8–S11. In order to predict the sensitivity of the device to refractive index variation of the surrounding medium, we perform a simulation to calculate the transmission spectrum by changing the refractive index of superstrate on nanoLCA. Figure 2c shows the simulated variation of transmission as a function of refractive index (RI) of surrounding medium. As observed in the experiment, the simulation results also showed red shift of both modes (SPP-BW and LSPR) with RI increase. The corresponding measured variation of transmission as a function of RI is shown in Figure 2d. The simulation results are strikingly similar with the experimental results about the appearance of two peaks and red shifting with the increase of RI.

In order to compare the sensitivity of nanoLCA, we measured the LSPR peak wavelength shift by precisely varying the concentration of NaCl solution. At low concentration (<1 mg mL^{-1} or 0.1% NaCl), with a difference of RI by 2 × 10^{-4} RIU (refractive index unit)[15] we observed wavelength shift of LSPR mode to be ~9 nm (**Figure 4**c), which corresponds to sensitivity of 46000 nm RIU^{-1}, exceeding all previously reported sensitivity by almost two order of magnitude (see Supporting comparison Table S1). An average sensitivity of 8066 nm RIU^{-1} (R^2 = 0.987) was achieved for higher concentration (>1 mg mL^{-1} or 0.1% NaCl) (Figure 4d). In order to compare the sensitivity of different metallic plasmonic sensors, a metric called figure of merit (FOM), $\frac{\Delta\lambda}{\Delta n}\left(\frac{1}{\Delta w}\right)$, where $\Delta\lambda$ is the amount of shift for the resonance peak wavelength for Δn is the change in the RI, Δw is the full-width-half-maximum (FWHM) of the peak in consideration, is widely used. We calculate a maximum FOM of ~1022 and an average FOM ~179 which far exceeds all reported FOM of nanohole structures (including the theoretical upper limit of FOM ~108 for gold standard SPR sensors;[15] metallic naoparticles has FOM ~0.9–5.4 and SPP structure has FOM ~ 23).[5,24] We assert that the high sensitivity is due to selective transmission of nanoparticle scattering light by the nanoLCA. There is also contribution from subradiant (long plasmon lifetime) SPP waves (at λ = 381 nm) (with a narrow full width at half maximum of 18 nm). Due to longer plasmon lifetime, the plasmon energy can be transferred to the emissive superradiant LSPR mode (at λ = 450 nm) (with FWHM of 48 nm) giving rise to further enhancement of local electric field. The corresponding bright-field image with different NaCl concentration is shown in Figure 4a. Typical spectrum for low concentration of NaCl solution is reported in Figure 4b. Transmission spectra obtained using other height (h = 1000 nm) and chemicals (glycerol, glucose, NaCl) are reported in Supporting Figure S12–S16.

To demonstrate the utility of nanoLCA for biosensing applications, we measured the hybridization of a short chain of probe oligonucleotides (5′-thiol-CAGCAAATGGGCTCCGAC-3′) and its perfectly matched target oligonucleotide (3′-GTCGGAGCCCATTTGCTG-5′-HEX). The 5′ end of the probe oligonucleotides was modified with a thiol group for ease of immobilizing on Ag surface. Our colorimetric SPR imaging technique does not require any label on the DNA, however, the target oligo was tagged with fluorophore HEX for independently verifying the hybridization in fluorescence mode. **Figure 5**a shows the detection of hybridization of oligonucleotides down to 100 pM through the BF imaging of nanoLCA. We are able to visualize the colorless DNA and able to differentiate the concentration of DNA based on the color change of the sensor device (raw images in Supporting Figure S17, S18). The transmission spectrum showed a red-shift of ~32 nm after DNA hybridization for the nanoLCA with h = 1000 nm (Supporting Figure S19).

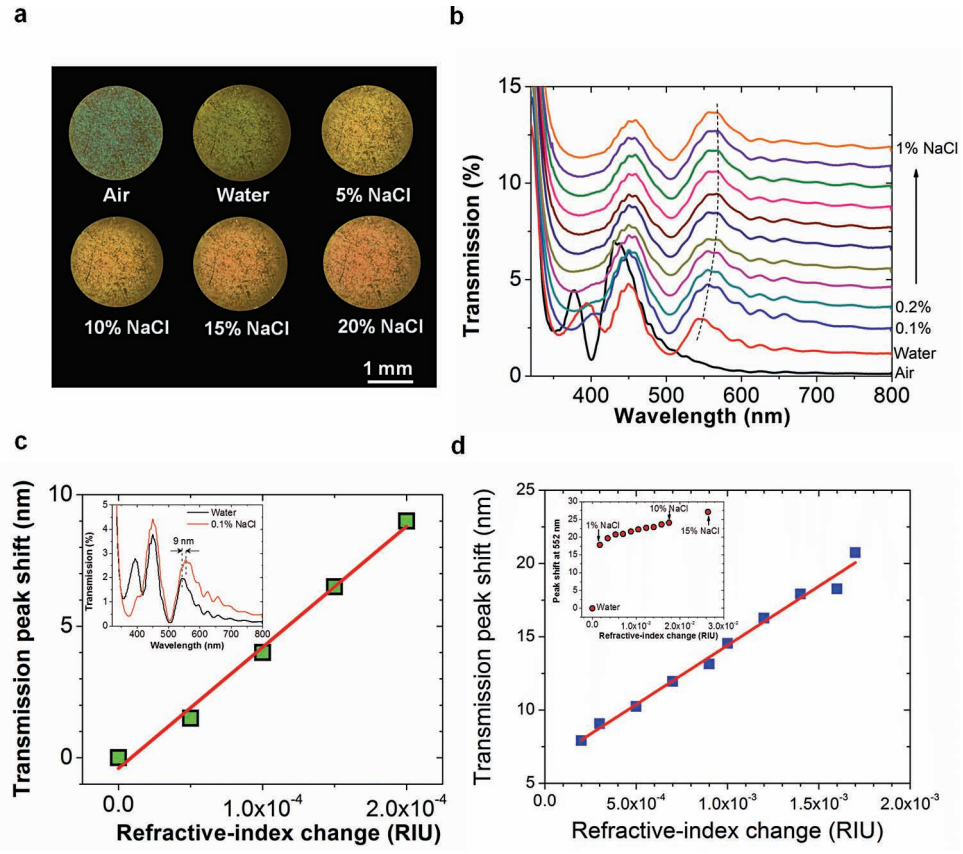

Figure 4. Refractive-index sensitivity and figure of merit of nanoLCA obtained using NaCl solution. (a) Optical micrograph of nanoLCA (h = 500 nm, t = 90 nm) with different concentration of NaCl solutions (0–20% by weight). (b) Transmission spectra of nanoLCA in presence of NaCl concentration of 0–1% with an increment of 0.1%. The LSPR resonance peak due to Mie scattering of nanoparticles along the sidewall (shown with dotted line) are red-shifted with change in NaCl concentration. (c) Sensitivity of nanoLCA calculated using a linear fitting scheme from the transmission spectra LSPR resonance peak shift obtained for NaCl concentration of 0–0.1% with an increment of 0.025%. The sensitivity was calculated to be 46,000 nm per RIU. (d) Sensitivity of nanoLCA calculated for Nal concentration range from 0–1%. The average sensitivity in high concentration range was calculated to be 8066 nm per RIU. The inset shows the LSPR resonance peak shift for nanoLCA for NaCl concentration range from 0–15%. The large peak shift at lower concentration clearly demonstrates that nanoLCA is more sensitive in lower concentration range.

As shown in Figure 5b, the hybridization of target oligonucleotide at 0.1 nM and 1 nM to the probe oligonucleotide resulted in approximately 1.9 and 2.1 times increase respectively in the intensity of the red channel compared to that of the negative control. Likewise, in the green channel, we observed approximately 3.3 and 4.3 times increase after the hybridization of the same concentrations of probe oligonucleotide. The difference in red channel intensity and EMD values are much more sensitive in lower concentration range compared to higher concentration, at which sensor is more likely saturating (confirming our earlier observation about RI-solution testing).

Furthermore, we performed a simple biomolecular protein-protein interaction experiment to demonstrate the therapeutic antibody screening functionality on nanoLCA. We are able to observe the color changes on the sensor surface (raw images in Supporting Figure S20) due to BSA/anti-BSA immune complex formation which is also relevant to the studies related to the receptor sites of red blood cells.[25] As shown in **Figure 6**a (top is red channel intensity, bottom is for green channel intensity), we can clearly discern between before and after immune complex formation for different concentration of BSA/anti-BSA from the nanoLCA imaging data (see Experimental Section and Supporting Figure S21). The spectral shift observed for the nanoLCA structure after BSA modification was ~42 nm (Supporting Figure S22). For a similar experiment, resonant wavelength shift of ~5 nm was observed,[20] which is 8.4 times lower than in the case of nanoLCA structure (even without optimization). In the colorimetric analysis, we observed a decrease in the intensity of the red and green channels following the BSA/anti-BSA complex formation. Further, in a previously reported experiment[15] using an EOT plasmonic structure, only reduction of transmitted intensities after antibody adsorption to the surface was observed (the color was changed from red (before protein incubation) to black (after protein incubation)). In contrast, nanoLCA leads to a change in color after protein adsorption due to the higher sensitivity of the device. The DNA and BSA experiments were performed in a 96-well microplate. We have also performed the experiment with microfluidics to show that nanoLCA can be integrated to a microfluidic device. Figure 6b shows the BF image of the nanoLCA sensor with a polydimethylsiloxane (PDMS) microfluidic on top of it. At the contact point of the PDMS to the surface of the nanoLCA sensor,

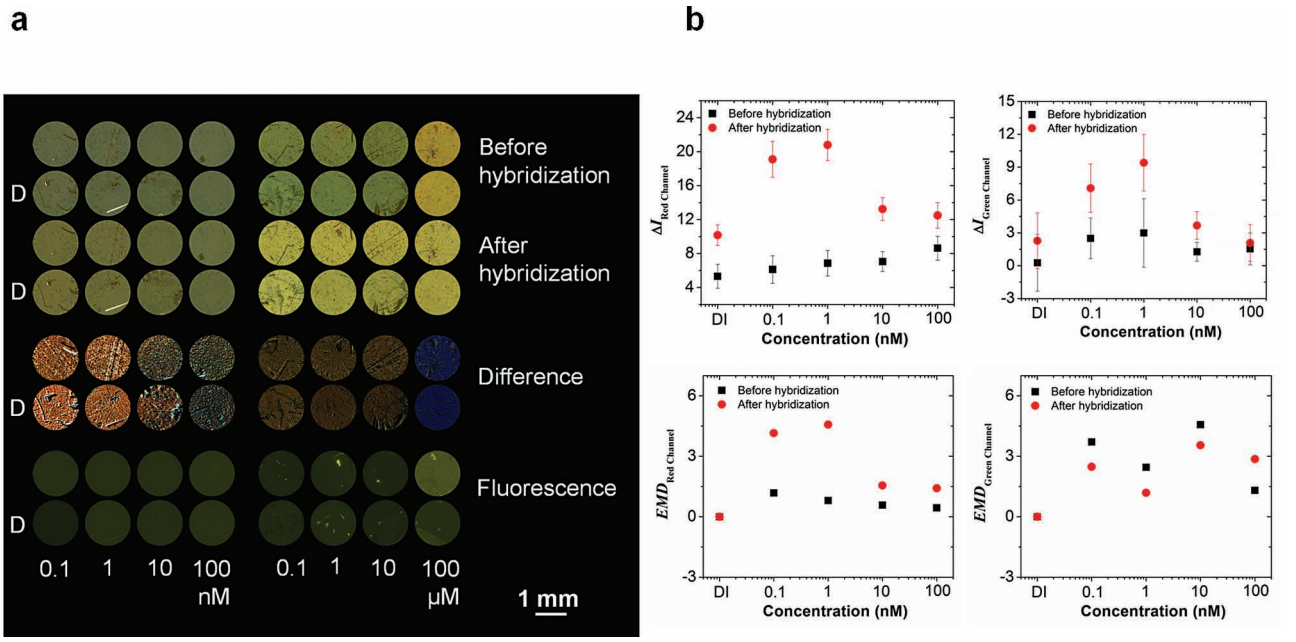

Figure 5. Detection of DNA hybridization on nanoLCA. (a) Bright field images of short chain oligonucleotides before and after hybridization. Here 'D' denotes duplicate experiments. The difference shows the direct subtraction of 'before hybridization' images from the 'after hybridization' images. Here, orange color (left) denotes higher count than blue color (right). (b) Variation of red and green channel intensity with different concentration of oligonucleotides before and after hybridization. The variation of EMD counts with concentration is also shown below for red and green channel respectively.

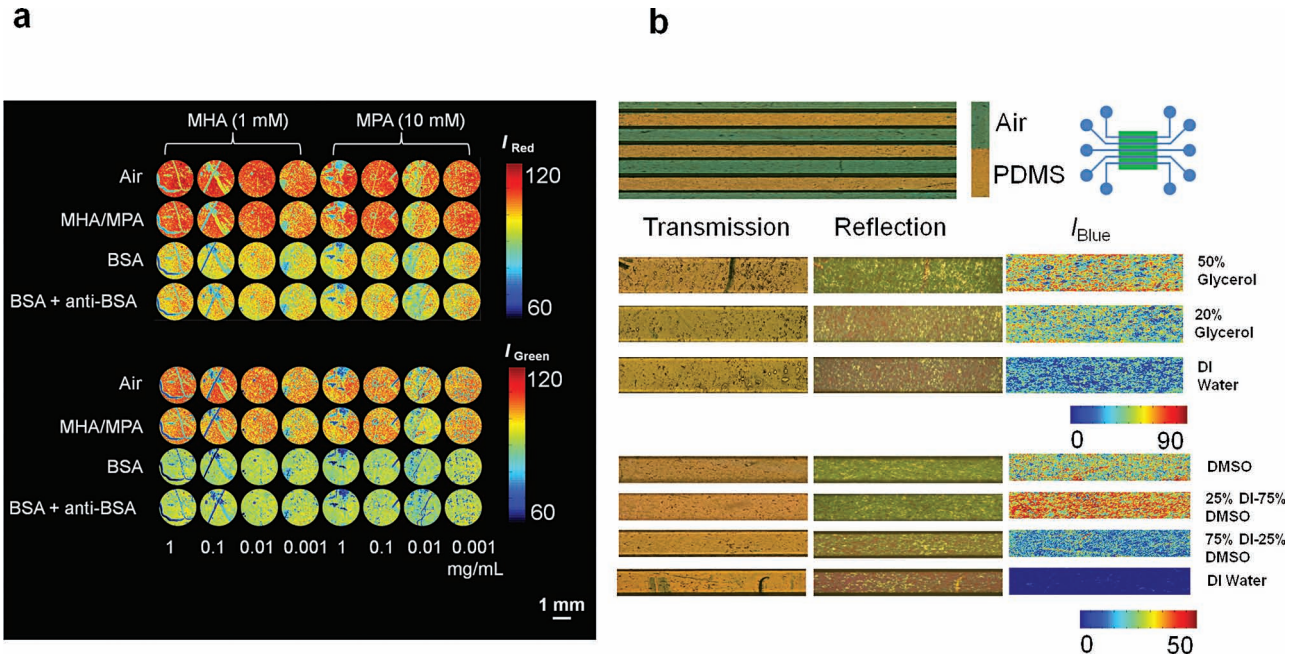

Figure 6. Biomolecular protein detection and microfluidics based sensing application using nanoLCA. (a) Variation of red channel (top) and green channel (bottom) intensity derived from the bright field images of nanoLCA coated with BSA (third and seventh row) and BSA+anti-BSA (fourth and eighth row). The images with air (first and fifth row) and MHA/MPA (second and sixth row) interfaces are also shown. The first four columns are for the cases when MHA (1 mM) is used for protein immobilization (0.001–1 mg/mL). The last four columns are the cases when MPA (10 mM) is used for protein immobilization (0.001–1 mg/mL) on nanoLCA surface. (b) Bright field transmission image of nanoLCA with a PDMS microfluidic device (schematically shown to the right) on top of it. The orange color is because of the PDMS in contact with the nanoLCA. The green color is for the empty microfluidics channel. The images below show the bright field transmission (left), reflection (middle) and blue channel intensities (right) of mixing experiments on nanoLCA with DI water-Gycerol (middle) and DI water-DMSO (bottom).

a color change is observed (green is in contact with air, red is in contact with PDMS). An added advantage of nanoLCA is that the proper contact of the device to the microfluidic surface can be checked even before the actual experiments. Figure 6b also shows the mixing experiments with glycerol-water and DMSO-water solution to demonstrate the gradient change in color due to different concentration of solutions in a microfluidic-on-nanoLCA environment.

In summary, we have developed a 'biochemical color camera' device mimicking Lycurgus cup effect to observe and perform quantitative biochemical sensing with unprecedented sensitivities. We have demonstrated the utility of the sensor for highly sensitive refractive-index sensing, DNA hybridization detection, protein-protein interaction and integration to portable microfluidics device for lab-on-chip applications. We envisage extensive use of the device for DNA microarrays, therapeutic antibody screening for drug discovery and pathogen detection in resource poor setting and a low cost, higher sensitive alternative to existing SPR/LSPR instruments.

Experimental Section

Fabrication of nanoLCA: The nanocone master made on glass substrate was passivated with dimethyl dichlorosilane solution for 30 min, followed by ethanol and deionized water rinse. This step promotes the formation of a hydrophobic silane layer on the master which helps in the removal of cured polymer replica. A 250 μm thick flexible (Poly)ethylene terephthalate (PET) sheet was used as a supporting substrate, and a Teflon roller was used for evenly distributing the UV curable polymer on the master and PET interface. In order to cure the UV polymer, a UV light-curing flood lamp system (Dymax EC-Series) with average power density of 105 mW cm^{-2} was used. The polymer was cured by UV light for 60 s at room temperature. For the metal (Ag, Au) evaporation a six pocket e-beam evaporation system (Temescal) was used. A thin adhesive layer of Titanium (5 nm) was deposited before the evaporation of Ag/Au.

Optical Characterization: NanoLCA transmission spectra were collected using Varian Cary 5G UV-Vis-NIR spectrophotometer (spectral bandwidth = 1 nm, data interval = 1 nm) with normal incidence transmission mode. The angle and polarization dependent transmission spectra were obtained by J.A. Woollam Co. variable angle spectroscopic ellipsometer. For the dispersion diagram (angle-wavelength), the transmission spectra were taken at 1° intervals. The reflectance spectra were obtained in an inverted microscope (Zeiss Axio Observer D1) equipped with 100 W halogen light source. The light was focused on to the sample with 20x objective (NA = 0.45) and the reflected light were collected by a silicon photodiode array (PDA) spectrometer (300–900 nm).

Image Analysis: The color images of the nanopore devices were captured using a transmission light microscope with 5x magnification (Olympus, Center Valley, PA, USA) with exposure time of 40 ms (gain = 1; gamma = 1). Each image is composed of three 8-bit channels of red, green, and blue, and therefore, each color image is 24-bit. For the calculation of mean intensity, an area of the 300 × 300 pixels (approximately 0.44 mm by 0.44 mm) was cropped from the original image to remove the boundary areas. The raw microscope images were splitted into three red, green, and blue (RGB) channels. The mean ($\mu = \sum_{i=1}^{N} x_i / \mu = \sum_{i=1}^{N} x_i\, NN$), standard deviation $\left(\delta = \left(\frac{1}{N-1}\sum_{i=1}^{N}(x_i-\mu)^2\right)^{1/2}\right)$, and mode of the intensity of the cropped area for each component were determined by the built-in MATLAB R2011b functions (MathWorks, Natick, MA, USA).

Earth's mover distance (EMD) algorithm was implemented to compute the flow that minimizes the overall ground distance between two signatures, S_A and S_B. Each signature, $S_x = \{(x_1,w_{x1}),...,(x_M,w_{xM})\}$, consists of m clusters with x_i, a cluster representative, and w_{xi}, the weight of the cluster. The distance, d_{ij}, is the vector norm (ground distance-) between clusters a_i and b_j. For each RGB channel, the signature consists of the binned (N = 100) intensity of the pixels in the cropped area and the weights of the bins, which were calculated as the number of pixels in the bin divided by the total number of pixels. In EMD calculation, the flow, f, between the clusters a_i and b_j, is calculated to minimize the overall work function: $WORK(A,B,F) = \sum_{i=1}^{M}\sum_{j=1}^{N} d_{ij}f_{ij}$. After the overall work function has been minimized, the EMD is calculated as: $EMD(A,B) = \sum_{i=1}^{M}\sum_{j=1}^{N} d_{ij}f_{ij} / \sum_{i=1}^{M}\sum_{j=1}^{N} d_{ij}f_{ij}\ \sum_{i=1}^{M}\sum_{j=1}^{N} f_{ij}\ \sum_{i=1}^{M}\sum_{j=1}^{N} f_{ij}$. In the EMD calculation of RGB images, the signature of DI water was compared to itself (as a negative control) and the signature of other dissimilar solutions.

FDTD Simulations: The 3D finite difference time-domain (FDTD) analysis was performed using a commercial software package (FDTD solutions, Lumerical Solutions, Inc. Vancouver, Canada). A unit magnitude plane wave with normal incidence angle, polarized in x-direction and propagating in +z direction was used for exciting the modes in nanoLCA. A uniform mesh size of 1 nm (x, y, z-directions) was used. The optical constants of Ag in the spectral range of 300-1100 nm were taken from Palik's handbook. In order to properly calculate the angular and wavelength dependent transmission spectra, perfectly matched layers (PMLs) are imposed at boundaries normal to the light propagation directions. Similarly, the boundary conditions in x and y directions were set as periodic.

Numerical Calculations: For the SPP-BW calculation, the dielectric constant of Ag is calculated with a Drude plus two-pole Lorentzian form as: $\varepsilon_{Ag}(\omega) = \varepsilon_\infty - \frac{\omega_D^2}{\omega^2 + i\gamma_D\omega} - \sum_{m=1}^{2}\frac{g_{L_m}\omega_{L_m}^2\Delta\varepsilon}{\omega^2 - \omega_{L_m}^2 + i2\gamma_{L_m}\omega}$ where, $\varepsilon_\infty = 2.3646$, $\omega_D = 8.7377\,eV$, $\gamma_D = 0.07489\,eV$, $\Delta\varepsilon = 1.1831$, $g_{L_1} = 0.2663$, $\omega_{L_1} = 4.3802\,eV$, $\gamma_{L_1} = 0.28\,eV$, $g_{L_2} = 0.7337$, $\omega_{L_2} = 5.183\,eV$ and $\gamma_{L_2} = 0.5482\,eV$. The Mie scattering calculation for the metal nanoparticles are performed using Lorenz–Mie theory (''MiePlot v 4.2.05'' by Philip Laven) (http://www.philiplaven.com/mieplot.htm).

Materials: The UV curable polymer (NOA 61) was obtained from Norland Products, Cranbury, NJ. Polydimethylsiloxane (PDMS) (Dow Corning, Midland, MI). Micro-channels were prepared using a 10:1 v/v ratio of base to curing agent and the polymer was cured at 65 °C for 1 h. Glycerol, NaCl and Glucose were purchased from Sigma and used without any modification. The custom made DNA sequences were obtained from Alpha DNA and used without any purification. The DNA was diluted with DI water for making different concentrations of DNA solution. For hybridization experiments, 1x Phosphate Buffer Solution (PBS) solution was used for the dilution of target DNA (HEX modified probe). Albumin from bovine serum (BSA), anti-bovine albumin (anti-BSA), *N*-hydroxysuccinimide (NHS) and *N*-(3-dimethylaminopropyl)-*N*′-ethylcarbodiimide hydrochloride (EDC) were obtained from Sigma-Aldrich.

DNA Hybridization Experiments: Two sets of DNA hybridization experiment were performed. In one experiment, the concentration of 'probe' DNA (5′-thiol-CAGCAAATGGGCTCCGAC-3′; hereafter called "DNA-1") was prepared from 100 nM to 100 μM and the concentration of 'target' DNA (3′-GTCGGAGCCCATTTGCTG-5′-HEX; hereafter called "DNA-2") was kept constant (10 μM). In the second experiment, concentration of DNA-1 was kept constant (100 nM) and the concentration of DNA-2 was prepared from 100 pM to 100 nM. The nanoLCA devices were first attached to the bottom of 96-well microplate (4 wells for the samples and 4 wells as duplicates). Transmission and reflection mode bright field (BF) images of each well were taken. Then 100 μL of DNA-1 solution (in DI water) was put in each well and imaged immediately. The DNA-1 solution was kept in a humidity controlled chamber for 24 h to allow the immobilization of oligo to the Ag surface through thiol chemistry. Images were taken after 24 h in wet state. The DNA-1 that is not bound to the surface was removed by washing thoroughly with DI water and the surface was dried by N_2 blow gun and immediately BF images were taken. Similarly, the nanoLCA devices were immersed in 100 μL of DNA-2 solutions, imaged immediately, incubated for 24 h, imaged again, washed and dried, and imaged subsequently, both in BF and fluorescence imaging mode.

Protein-Protein Binding Experiments: In order to make carboxylated monolayer and thiol linker on the surface, 3-mercaptopropionic acid

(MPA) (10 mM) and 6-mercaptohexanoic acid (MHA) (1 mM) in anhydrous ethanol solution were used. Immobilization of protein (BSA) to the surface was achieved by linking one of the amine functional groups on protein to the carboxyl group through a peptide bond (amide linkage) in the presence of catalyst EDC (50 mM) and NHS (200 mM). Different concentrations of BSA solution (0.001 –1 mg/mL) were prepared in DI water. The concentration of anti-BSA solution prepared in 1x phosphate buffered saline (PBS) was kept constant (0.01 mg/mL). Images were taken at each step (before addition of solution, after addition of solution and after washing and drying).

Supporting Information

Supporting Information is available from the Wiley Online Library or from the author.

Acknowledgements

The authors thank Jing Jiang and Te-Wei Chang for help with the SEM. We thank Hoang Nguyen, Cindy Larson for the preparation of master nanopillar mold. Transmission experiments were carried out in the Frederick Seitz Materials Research Laboratory Central Facilities, University of Illinois, which are partially supported by the U.S. Department of Energy under Grants DE-FG02-07ER46453 and DE-FG02-07ER46471.

Received: October 4, 2012

[1] U. Leonhardt, *Nat. Photonics* **2007**, *1*, 4.
[2] W. A. Murray, W. L. Barnes, *Adv. Mater.* **2007**, *19*, 22.
[3] M. E. Stewart, C. R. Anderton, L. B. Thompson, J. Maria, S. K. Gray, J. A. Rogers, R. G. Nuzzo, *Chem. Rev.* **2008**, *108*, 2.
[4] a) S. Lal, S. Link, N. J. Halas, *Nat. Photonics* **2007**, *1*, 11; b) H. Chen, X. Kou, Z. Yang, W. Ni, J. Wang, *Langmuir* **2008**, *24*, 5233; c) D. P. Lyvers, J. M. Moon, A. V. Kildishev, V. M. Shalaev, A. Wei, *ACS Nano* **2008**, *2*, 2569; d) S. Zhang, K. Bao, N. J. Halas, H. Xu, P. Nordlander, *Nano Lett.* **2011**, *11*, 1657.
[5] a) J. N. Anker, W. P. Hall, O. Lyandres, N. C. Shah, J. Zhao, R. P. Van Duyne, *Nat. Mater.* **2008**, *7*, 6; b) N. Ahamad, A. Bottomley, A. Ianoul, *J. Phys. Chem. C* **2012**, *116*, 185; c) S. J. Zalyubovskiy, M. Bogdanova, A. Deinega, Y. Lozovik, A. D. Pris, K. H. An, W. P. Hall, R. A. Potyrailo, *J. Opt. Soc. Am. A* **2012**, *29*, 994; d) C. Qian, C. Ni, W. Yu, W. Wu, H. Mao, *Small* **2011**, *7*, 1801.
[6] T. W. Ebbesen, H. J. Lezec, H. F. Ghaemi, T. Thio, P. A. Wolff, *Nature* **1998**, *391*, 6668.
[7] M. E. Stewart, N. H. Mack, V. Malyarchuk, J. A. N. T. Soares, T. Lee, S. K. Gray, R. G. Nuzzo, J. A. Rogers, *Proc. Natl. Acad. Sci. USA* **2006**, *103*, 46.
[8] N. Ganesh, W. Zhang, P. C. Mathias, E. Chow, J. A. N. T. Soares, V. Malyarchuk, A. D. Smith, B. T. Cunningham, *Nat. Nanotechnol.* **2007**, *2*, 8.
[9] F. Vollmer, S. Arnold, *Nat. Methods* **2008**, *5*, 7.
[10] I. D. Block, L. L. Chan, B. T. Cunningham, *Sens. Actuat. B-Chem.* **2006**, *120*, 1.
[11] A. J. Haes, R. P. Van Duyne, *Anal. Bioanal. Chem.* **2004**, *379*, 7–8.
[12] S. Roh, T. Chung, B. Lee, *Sensors* **2011**, *11*, 2.
[13] A. V. Kabashin, P. Evans, S. Pastkovsky, W. Hendren, G. A. Wurtz, R. Atkinson, R. Pollard, V. A. Podolskiy, A. V. Zayats, *Nat. Mater.* **2009**, *8*, 11.
[14] C. Genet, T. W. Ebbesen, *Nature* **2007**, *445*, 7123.
[15] A. A. Yanik, A. E. Cetin, M. Huang, A. Artar, S. H. Mousavi, A. Khanikaev, J. H. Connor, G. Shvets, H. Altug, *Proc. Natl. Acad. Sci. USA* **2011**, *108*, 29.
[16] a) M. R. Gartia, Z. Xu, E. Behymer, H. Nguyen, J. A. Britten, C. Larson, R. Miles, M. Bora, A. S. Chang, T. C. Bond, G. L. Liu, *Nanotechnol.* **2010**, *21*, 39; b) Z. Xu, H. Y. Wu, S. U. Ali, J. Jiang, B. T. Cunningham, G. L. Liu, *J. Nanophoton.* **2011**, *5*, 053526.
[17] A. Fernandez, H. T. Nguyen, J. A. Britten, R. D. Boyd, M. D. Perry, D. R. Kania, A. M. Hawryluk, *J. Vac. Sci. Technol. B* **1997**, *15*, 3.
[18] H. Chen, T. Ming, L. Zhao, F. Wang, L. Sun, J. Wang, C. Yan, *Nano Today* **2010**, *5*, 5.
[19] P. Chaturvedi, K. H. Hsu, A. Kumar, K. H. Fung, J. C. Mabon, N. X. Fang, *ACS Nano* **2009**, *3*, 10.
[20] A. G. Brolo, R. Gordon, B. Leathem, K. L. Kavanagh, *Langmuir* **2004**, *20*, 12.
[21] J. M. McMahon, J. Henzie, T. W. Odom, G. C. Schatz, S. K. Gray, *Opt. Express* **2007**, *15*, 26.
[22] T. Xu, H. Shi, Y. Wu, A. F. Kaplan, J. G. Ok, L. J. Guo, *Small* **2011**, *7*, 22.
[23] J. Yang, H. Gao, J. Y. Suh, W. Zhou, M. H. Lee, T. W. Odom, *Nano Lett.* **2010**, *10*, 8.
[24] J. Henzie, M. H. Lee, T. W. Odom, *Nat. Nanotechnol.* **2007**, *2*, 9.
[25] L. Varga, E. Thiry, G. Fust, *Immunology* **1988**, *64*, 3.